Advancing the Growth of GaN on AlScN and AlYN by Metal–Organic Chemical Vapor Deposition

Isabel Streicher,* Niklas Wolff, Teresa Duarte, Oliver Rehm, Patrik Straňák, Lutz Kirste, Mario Prescher, Xuyun Guo, Valeria Nicolosi, Lutz Baumgarten, Martina Müller, Lorenz Kienle, and Stefano Leone*

High electron mobility transistors (HEMT) based on $Al_{1-x}Sc_xN$/GaN and $Al_{1-x}Y_xN$/GaN heterostructures promise increased device performance and reliability due to the high sheet charge carrier density and the possibility to grow strain-free layers on GaN. Metal–organic chemical vapor deposition (MOCVD) offers high throughput, high structural quality, and good electrical characteristics. The growth of GaN layers on $Al_{1-x}Sc_xN$ and $Al_{1-x}Y_xN$ is challenging, but at the same time crucial as passivation or for multichannel structures. GaN is observed to grow three-dimensionally on these nitrides, exposing not-passivated areas to surface oxidation. In this work, growth of 2–20 nm-thick, two-dimensional GaN layers is demonstrated. Optimization of growth conditions is enabled by understanding island formation on the atomic scale by aberration corrected scanning transmission electron microscopy (STEM) and hard X-ray photoelectron spectroscopy (HAXPES). Increased growth temperature, an AlN interlayer, low supersaturation conditions and the carrier gas are found to be key to enhance Ga adatom mobility. Growth of single crystalline GaN layers on $Al_{1-x}Sc_xN$ and $Al_{1-x}Y_xN$ is unlocked and prevents oxidation of the underlying layers. Few nanometer thick GaN caps allow for depositing the gate metallization directly on the cap, whereas thicker ones allow for the growth of heterostructures for normally-off devices and multichannel structures.

1. Introduction

A sustainable future demands for energy savings in data transmission, from smart devices to radar and satellites, and efficient conversion of electricity in inverters and converters, which are present for example in photovoltaic systems and electric vehicles. AlGaN/GaN high-electron mobility transistors (HEMT) offer high switching frequencies, high breakdown voltages, and are capable to handle high current densities.[1,2] However, there are intrinsic limits posed by the number of charge carriers in the polarization-induced two-dimensional electron gas (2DEG) at the AlGaN/GaN interface and lattice-mismatch induced strain compromises the lifetime of devices.[3] The sheet charge carrier density n_s of the 2DEG can be increased by using $Al_{1-x}Sc_xN$ or $Al_{1-x}Y_xN$ as barrier layers. The high spontaneous polarization of these materials increases the n_s by up to a factor of five, depending on their composition.[4,5] The high n_s enables the switching of

I. Streicher[+], T. Duarte, P. Straňák, L. Kirste, M. Prescher, S. Leone
Fraunhofer Institute for Applied Solid State Physics (IAF)
Tullastrasse 72, Freiburg D-79108, Germany
E-mail: isabelmariastreicher@gmail.com;
stefano.leone@iaf.fraunhofer.de

N. Wolff, L. Kienle
Department of Material Science
Kiel University
Kaiserstr. 2, Kiel D-24143, Germany

N. Wolff, L. Kienle
Kiel Nano, Surface and Interface Science (KiNSIS)
Kiel University
Christian-Albrechts-Platz 4, Kiel D-24118, Germany

O. Rehm, M. Müller
Department of Physics
Universität Konstanz
Konstanz D-78457, Germany

X. Guo, V. Nicolosi
School of Chemistry
Centre for Research on Adaptive Nanostructures and Nanodevices (CRANN)
Advanced Materials Bio-Engineering Research Centre (AMBER)
Trinity College Dublin
Dublin Dublin 2, Ireland

L. Baumgarten
Forschungszentrum Jülich GmbH
Peter Grünberg Institut (PGI-6), Jülich D-52425, Germany

higher currents in power transistors, while power amplifiers profit from the higher output powers achieved at Ka-band frequencies (30 GHz). The fact that both $Al_{1-x}Sc_xN$ or $Al_{1-x}Y_xN$ are high-k dielectrics promises for decreased electron tunneling and leakage currents without losses in gate capacitance.[6,7] The first MOCVD-grown $Al_{1-x}Sc_xN$/GaN HEMTs, grown with a SiN_x cap, exhibit the highest reported combination of output power P_{out} and a power added efficiency PAE at 30 GHz reported for class-AB continuous wave operation at Ka-band frequencies on metal-polar GaN-based HEMTs so far. The achieved P_{out} was 8.4 W/mm and the PAE was 42.0 %, respectively.[8] Both $Al_{1-x}Sc_xN$ and $Al_{1-x}Y_xN$ feature an a lattice parameter matching with that of GaN, thus allowing the growth of strain-free barriers, potentially increasing the lifetime of devices. The exact concentrations at which the lattice matching occurs are a subject of discussion. Recent evidence point at a Sc concentration of 9, 11, or 14%,[9–11] and a Y concentration of 8%, respectively.[5,12]

$Al_{1-x}Sc_xN$ and $Al_{1-x}Y_xN$ are very susceptible to oxidation, due to the low standard redox potentials of both Sc and Y.[13] This leads to surface oxidation as soon as the layers are exposed to air, which can lead to an oxide layer on the sample surface[14–16] and even decomposition.[17] The role of oxygen in wurtzite $Al_{1-x}Sc_xN$ is yet unclear, analogue to oxygen in GaN and ScN, it is expected to act as electron donor.[18–20] 10 nm - thick SiN_x caps were employed successfully as surface passivation layer.[8,21,22] While SiN_x protects the barrier from oxidation, it needs to be opened locally for the deposition of the gate metal when HEMTs are fabricated, exposing the barrier not only to oxidation but also to damage induced by the dry etching, for example, by SF_6. In contrast, few nm - thick GaN caps protect the $Al_{1-x}Sc_xN$ surface from oxidation and allow the direct deposition of the gate metal. GaN caps influence the depth of the potential well and the n_s of the 2DEG. If they exceed a certain thickness, 2D hole gases form inside the GaN cap.[23,24] GaN caps doped with magnesium can be employed as gates for normally-off HEMTs.[25] Ultimately, multiple GaN/barrier stacks placed on top of each other are a very promising approach to fabricate HEMTs with decreased channel resistance and enhanced transport properties.[26] Lattice-matched GaN/AlScN multichannel structures allow for an unlimited number of barrier/channel pairs and promise for higher lifetimes of devices.[10]

Metal–organic chemical vapor deposition (MOCVD) is the growth method preferred by industry for high throughput, low maintenance cost and at the same time high structural quality of the epilayers. Growth of GaN caps by MOCVD is challenging regardless of the barrier material as GaN layers tend to decompose at high growth temperatures, which are however needed to favor Ga-adatoms mobility. Back-etching can lead to the formation of pits or even the complete removal of the GaN cap when the layer surface is not stabilized sufficiently by NH_3 during the cool-down from growth to room temperature.[27–29] The growth of GaN on Sc-containing layers seems to be limited by additional mechanisms that favor island growth.[21,30]

In this work, we demonstrate how continuous GaN layers can be grown by MOCVD on $Al_{0.94}Sc_{0.06}N$ and $Al_{0.92}Y_{0.08}N$ layers by choosing an appropriate spatial separation of the nitride barrier and the GaN cap and by tuning the growth temperature and gas flows. We reveal Sc- and Y-rich surface termination using the analytical combination of scanning transmission electron microscopy (STEM) and hard X-ray photoelectron spectroscopy (HAXPES), which are accounted for initially promoting island growth alongside the growth conditions. We show outstanding structural quality of $Al_{0.94}Sc_{0.06}N$ barriers and the GaN layers with HRSTEM. Electron energy loss spectroscopy investigations confirms that sufficiently thick GaN caps can prevent oxidation of the barrier layer interface. Using the combination of STEM-EELS and HAXPES, details of the buried interface chemistry of $Al_{1-x}Sc_xN$ /GaN heterostructures are revealed element-selectively by surface and bulk-sensitive measurements of core levels. The presence of 2DEGs in the GaN capped $Al_{1-x}Sc_xN$/GaN heterostructures was confirmed with capacitance–voltage (C–V) measurements. The investigated $Al_{1-x}Y_xN$/GaN, in contrast, suffers from compositional segregation that is probably responsible for the poor electrical performance in C–V measurements.

2. Results and Discussion

An analysis of GaN islands formed on $Al_{1-x}Sc_xN$ layers, as previously reported by Manz et al. is discussed in Section 2.1. The importance of a GaN passivation layer to prevent oxidation is presented in the following Section 2.2. Eventually, the mechanism to achieve a 2D GaN layer on top of AlScN layer is presented in Section 2.3, while a fine tuning of the morphology by tuning the supersaturation is explained in Section 2.4. Finally smooth and uniform AlScN/(AlN)/GaN heterostructure are illustrated in Section 2.5, while the growth of GaN on AlYN is shortly discussed in the last section 2.6.

2.1. GaN Islands

GaN tends to form islands when grown on layers of $Al_{1-x}Sc_xN$, but the influence of interface chemistry on the growth mechanisms are not yet fully understood.[21,30] In a prior study, we evidenced a change of interface chemistry by observing strong Sc-intermixing at the interface of capped SiN_x/$Al_{1-x}Sc_xN$ systems.[31] It was attributed to Sc residuals in the gas lines that, because of the considerable distance between the reactor inlet valve and the reactor chamber, lead to an excess of Sc precursor in the reactor chamber after the growth of $Al_{1-x}Sc_xN$ was nominally completed. While the Sc residuals in the SiN_x cap were removed by reducing the showerhead cooling temperature and proper growth conditions, HAXPES and HRSTEM investigations reveal that vertically and horizontally homogeneous $Al_{1-x}Sc_xN$ barriers are still terminated by a one or two atomic layers thin Sc-rich interface, which could facilitate GaN island growth, see **Figure 1**. We assume that Ga adatoms suffer of a lower mobility in the presence of Sc in the AlN matrix. Although we exclude a binding of Ga to Sc atoms, it may be that Sc creates some lattice distortion that hinders the mobility of Ga-atoms, or that N-atoms bond to Sc have a different binding energy to Ga, making it slower on the surface.

Herein, HAXPES allows for an adequate energy resolution that allows to detect minor changes in the electronic and chemical structure in the order of below 100 meV, providing integrated information on the entire dimensions of the photon beam (see also schematics in **Figure 2f**). In addition, analytical STEM is a capable method of investigating crystalline and chemical structures
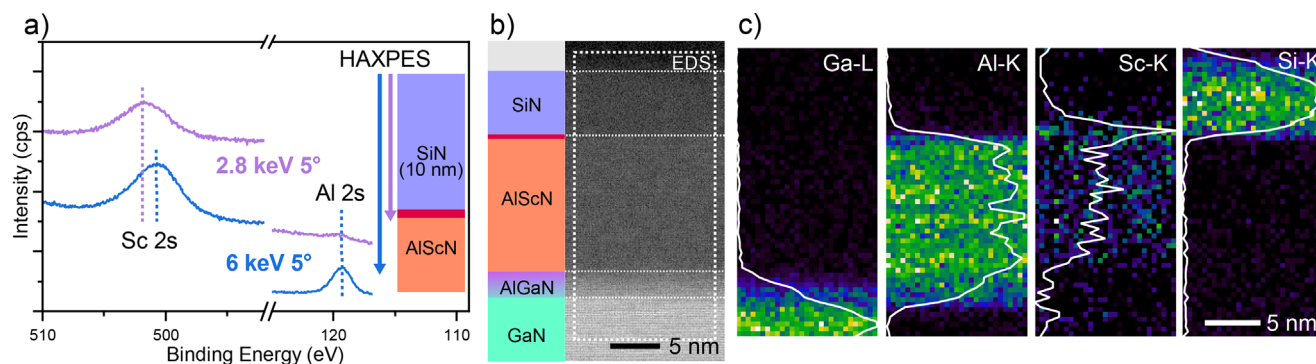
**ADVANCED
SCIENCE NEWS**

www.advancedsciencenews.com

**ADVANCED
PHYSICS
RESEARCH**

www.advphysicsres.com

Figure 1. Combined HAXPES and STEM-EDS measurements reveal an altered interface chemistry in SiN_x capped $Al_{1-x}Sc_xN$/GaN heterostructures, showing that the vertically chemically homogeneous barrier is terminated by a Sc-enriched layer. The interface of the $Al_{0.94}Sc_{0.06}N$ barrier with the GaN channel shows the characteristic transition from $Al_{0.94}Sc_{0.06}N$ to GaN via a few nm-thick graded $Al_{1-x}Ga_xN$ layer that we reported on in our previous works.[31,32] a) HAXPES measurements at different photon energies. b) Scheme of the heterostructure and HRSTEM image. c) EDS maps showing the distribution of the Ga-L, Al-K, Sc-K and Si-K signal intensities.

with sub-nanometer resolution. Figure 1a presents the HAXPES signatures of an $Al_{0.94}Sc_{0.06}N$ layer with a 10 nm SiN_x capping layer, measured at photon energies of 2.8 keV and 6 keV. Due to its lower information depth (ID), the measurement at 2.8 keV provides information about the $Al_{0.94}Sc_{0.06}N$ layer near the SiN_x/$Al_{0.94}Sc_{0.06}N$ interface, while the 6 keV measurement, with an ID approximately twice that of 2.8 keV, has a larger ID and contains information on the bulk-like $Al_{0.94}Sc_{0.06}N$ layer. All

details on IDs and energy resolutions of the HAXPES spectra are provided in the Methods section.

In the 2.8 keV (more interface-sensitive) spectra, the recorded intensity of the Al 2s peak feature is barely higher than the measurements detection limit, while in the 6 keV spectra the Al 2s peak is well resolved. In contrast, the Sc 2s peak is visible in both the 2.8 and 6 keV spectra, with no significant change in peak intensity.
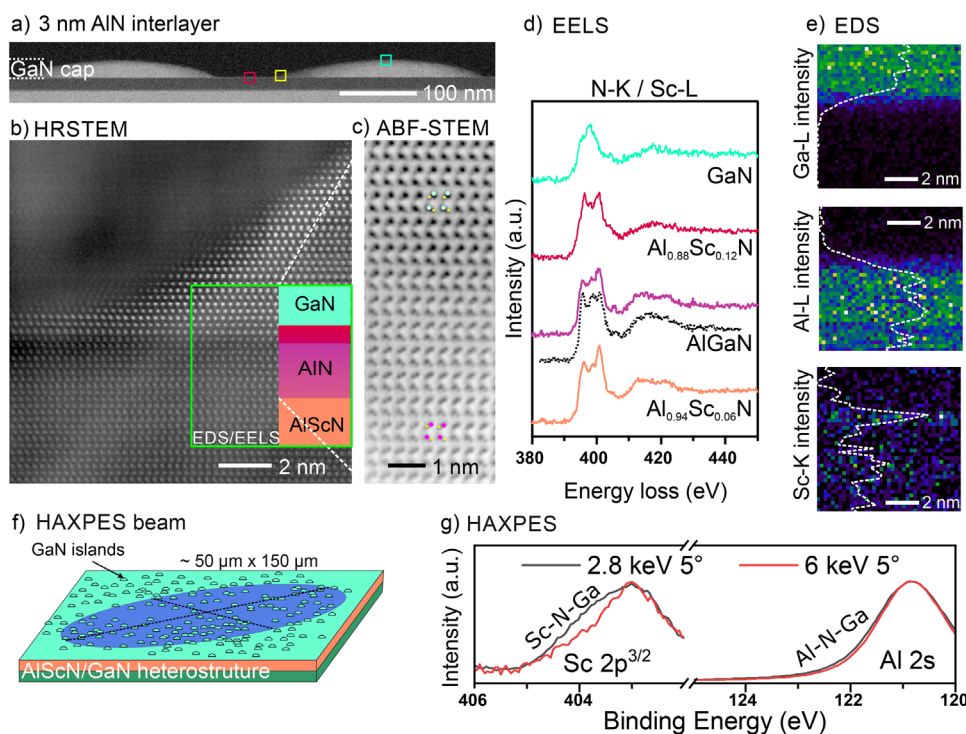

Figure 2. STEM analysis of $Al_{1-x}Sc_xN$/GaN heterostructures grown with a nominal 3 nm AlN interlayer between the $Al_{0.94}Sc_{0.06}N$ barrier and GaN cap showing island growth a) HAADF-STEM overview image. The colored squares indicate measurement areas. b) Atomic resolution HRSTEM image of the $Al_{1-x}Sc_xN$/GaN heterostructures interface region from the yellow area. c) ABF-HRSTEM image of the unit cell polarity across the interface. d) EELS analysis of ELNES signals of the convoluted N-K and Sc-$L_{2,3}$ transitions. e) EDS maps and intensity profiles of Ga-L, Al-L and Sc-K signals. f) Sketch of the HAXPES measurement geometry averaging over the GaN monolayers and island covered surface. g) Surface and bulk sensitive HAXPES measurements of core-level binding energies recorded at 2.8 and 6 keV, respectively.

**ADVANCED
SCIENCE NEWS**

www.advancedsciencenews.com

**ADVANCED
PHYSICS
RESEARCH**

Open Access

www.advphysicsres.com

These observed intensity variations for Al and Sc cannot be attributed to changes in photoionization cross-sections at different core levels and excitation energies. Both Sc 2s and Al 2s exhibit a comparable decrease in cross-section by a factor of about 1/6 and 1/7.7 with increasing the excitation energy to 6 keV.[33] For a homogeneous $Al_{0.94}Sc_{0.06}N$ layer, this should result in similar intensity scaling for both Sc 2s and Al 2s. However, this is not observed, indicating that the $Al_{0.94}Sc_{0.06}N$ layer is chemically not uniform. Instead, an enrichment of Sc at the $SiN/Al_{0.94}Sc_{0.06}N$ interface is expected. Congruently, a Sc-enriched layer terminating the $Al_{0.94}Sc_{0.06}N$ barrier is confirmed by STEM-EDS measurements displayed in Figure 1b,c showing a cross-section of the $Al_{1-x}Sc_xN/GaN$ heterostructures and corresponding elemental maps. The elemental profiles demonstrate the formation of an unintentionally graded ternary $Al_{1-x}Ga_xN$ layer at the GaN channel and a sharp peak in the Sc-K signal at the $SiN/Al_{0.94}Sc_{0.06}N$ interface, which forms by interdiffusion of atoms at high growth temperatures. This has been studied in detail in our previous works.[31,32]

To reduce the possible influence of the Sc-enriched interface chemistry, a nominal 3 nm AlN interlayer was grown without interruption after the $Al_{0.94}Sc_{0.06}N$ barrier layer to spatially separate the Sc-enriched layer from the GaN cap. AlN interlayers were shown to induce compositional grading at the barrier and channel interface, improving the abruptness of the interface and the 2DEG confinement also at very high thermal budgets.[31,32] However, the nominal AlN interlayer did not prevent the formation of GaN islands as large as 230 nm in diameter and 25 nm in height as visible from the AFM image shown in the Supporting Information (Figure S1). HRSTEM investigation of the GaN-capped $AlN/Al_{1-x}Sc_xN/GaN$ heterostructures shows the Sc-rich termination layer is still present at the interface to the GaN layer. The heterostructure morphology is displayed in the cross-section STEM and HRSTEM images presented in Figure 2a,b showing that the barrier layer is indeed covered by two to three monolayers of GaN in-between the islands. Atomic resolution ABF-STEM is sensitive to image atomic columns containing light atoms such as nitrogen. Analysis of the metal(M)-nitrogen dumbbell orientation across the heterostructure reveals the conservation of the M-polarity across the GaN/barrier interface as shown in Figure 2c. Combined spectroscopic analysis via EELS and EDS was conducted on the interface structure by acquiring both signals simultaneously. The spectral lines of the N-K and $Sc - L_{2,3}$ transitions are convoluted in the electron energy loss near edge structures (ELNES) shown in Figure 2d. Despite the convoluted fine structure, we observe a strong sensitivity to the Sc concentration within the $Al_{0.94}Sc_{0.06}N$ barrier layer in the low Sc concentration range. This is because the strong white-line features of the $Sc-L_{2,3}$ transition originates from the sharp and defined transitions from the $2p_{3/2}$ and $2p_{1/2}$ levels into unoccupied 3d-states ($L_{2,3}$) present for the transition metals, which influence becomes exceedingly visible for concentrations below 15 at.%, before becoming the dominant signal contribution. This is reflected in the normalized signals of the displayed ELNES showing small variations of the double-peak intensities for each layer. By taking the signal from the $Al_{0.94}Sc_{0.06}N$ layer as a benchmark for $x = 0.06$, less Sc is expected within the nominal AlN interlayer showing more individual fine structure from the pure N-K transition as ob-

served within the graded $Al_{1-x}Ga_xN$ layer (dashed line). In contrast, the ELNES signal recorded between the nominal AlN interlayer and the GaN island shows a more pronounced contribution of Sc suggesting an Sc-enriched interface with $x > 0.06$. These observations are confirmed by the simultaneously recorded EDS signals shown in Figure 2e), concluding on minor doping of the AlN interlayer with Sc and the presence of a Sc-rich $Al_{1-x}Sc_xN$ termination interfacing the GaN cap.

Figure 2f presents the normalized HAXPES spectra of the GaN island-capped $Al_{0.94}Sc_{0.06}N$ layer. In both the 2.8 and 6 keV measurements, the Sc $2p_{3/2}$ and Al 2s core levels are clearly resolved and show no significant intensity changes. By adding cross-section correction to the raw data intensities, we conclude on an enrichment of Sc atoms at or close to the surface: For the 2.8 keV measurement, a 14% higher Sc concentration is determined compared to the more bulk-sensitive measurement at 6 keV. This finding is consistent with the EDS measurement showing an Sc-enriched interface layer (compare Figure 2e).

Furthermore, a comparison of the normalized peak shapes provides insights into the chemical composition of the material. Both Sc 2p and Al 2s peaks exhibit a shoulder at higher binding energies relative to the maxima intensity. The main peaks correspond to Sc-N and Al-N bonds, respectively, while the shoulders represent Sc-N-Ga and Al-N-Ga bonds. The more pronounced peak shoulder for Sc $2p_{3/2}$ compared to Al 2s is attributed to the Sc enrichment at the GaN interface, as discussed before.

Due to the larger electronegativity of Ga compared to Al and Sc, the X-N-Ga spectral component (X = Al, Sc), is located at higher binding energies for Al and Sc core levels, while for Ga, the X-N-Ga component should appear at lower binding energies. For Ga $3p_{3/2}$, this shoulder is below the detection limit. The relatively small effect for Ga can be explained by the fact that the HAXPES beam spot (50 μm × 150 μm) averages over the bulk-like ~25 nm thick GaN islands, which have diameters in the range of hundreds of nanometers and the free surface which is covered by only three monolayers of oxidized GaN. Therefore, the HAXPES measurement yields a strong Ga signal intensity from bulk-like islands, with minimal contribution from the interface, making an observation of the X-N-Ga component in Ga $3p_{3/2}$ almost negligible.

2.2. Surface Oxidation

The GaN capping layer thickness is crucial to prevent the surface oxidation of Sc- and Y-containing barrier layers, since these transition metals are prone to oxidation.[14–16] In Figure S2 (Supporting Information) we show analytical STEM analysis performed on the monolayer GaN cap in-between the islands and on the top of the GaN islands using EDS and EELS. The presence of oxidized interface layers was detected at both regions. In case of the monolayer GaN cap, the interdiffusion of the GaN monolayers with the Sc-rich termination layer during high-temperature GaN growth is evidenced. As consequence of oxidation, the EDS and EELS data show a locally confined oxide layer which does not reach into the Sc-poor nominal AlN layer underneath. Without the presence of Sc at the surface of the GaN islands, we found traces of oxygen within the first 3–5 nm of the GaN island. Hence,
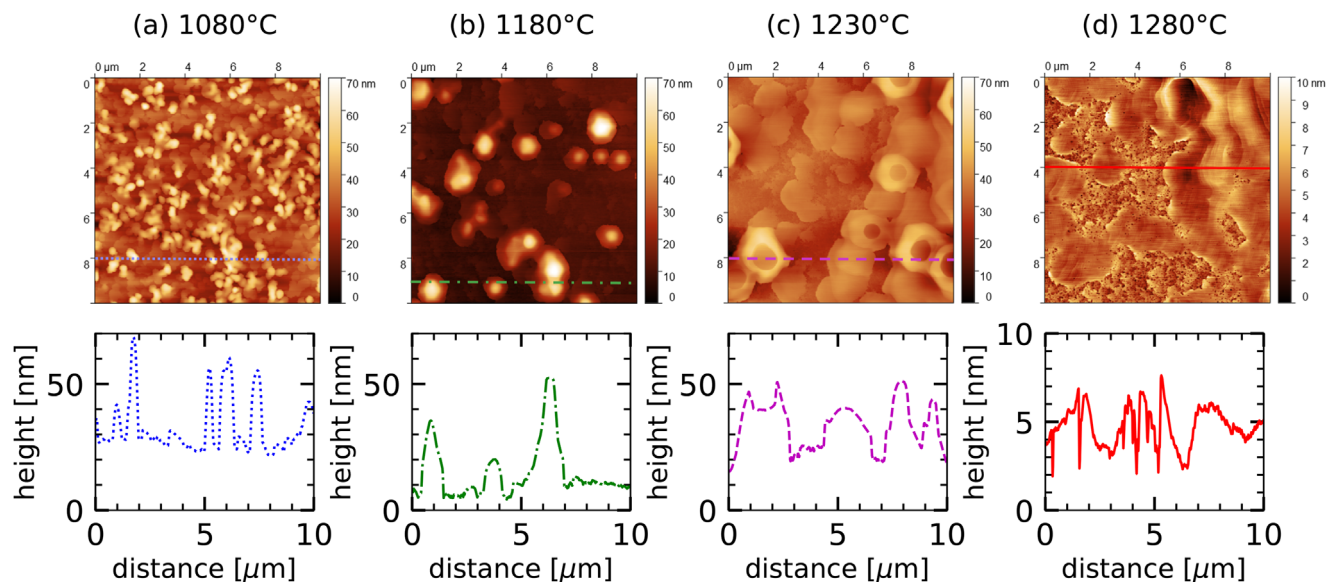
**ADVANCED
SCIENCE NEWS**

www.advancedsciencenews.com

**ADVANCED
PHYSICS
RESEARCH**

www.advphysicsres.com

Figure 3. AFM images (10 × 10 μm) and height profiles of GaN caps grown at a) 1080 °C, b) 1180 °C, c) 1230 °C and d) 1280 °C, respectively. All GaN caps were grown on the AlScN barriers after the reactor was baked. Furthermore an AlN was inserted between barrier and cap. Note that the height scale in (d) is significantly reduced.

providing a decently thick GaN cap can prevent oxidation of the electronic barrier layer and its interfaces.

2.3. Growth Temperature

Thin AlN interlayers inserted between the AlScN barrier and the GaN cap alone are not sufficient to remove the Sc-enriched layer at the top of the cap and suppress the 3D growth of the GaN cap, as shown before. A combination of the AlN interlayer with desorption steps, including a growth interruption with a bake and cleaning of the reactor chamber, and increased growth temperature of the GaN layer lead to significant improvement in the surface morphology. As shown in **Figure 3a**, the GaN cap displays a very rough surface when grown at 1080°C with a RMS value of 9.42 nm in the 10x10μm scans. An increase of the growth temperature to 1180°C led to a reduction of the number of GaN islands to fewer larger ones, as shown in the AFM image, as shown in Figure 3b. The surface roughness remained high with 10.5 nm. The coalescence of GaN islands increased further with the increase of the growth temperature of the GaN cap to 1230°C. The RMS value reduced to 6.28 nm. A crater-like morphology was observed for some GaN islands as shown in Figure 3c. A smooth surface was finally achieved at a growth temperature of 1280 °C. Apparently this high temperature is crucial to increase Ga-adatoms mobility and achieve a lateral growth mechanism. The RMS value of the 10x10 μm scan dropped to 1.12 nm. Growth steps of the GaN surface are visible. Local back-etching features are observed.

When N_2 instead of H_2 is used as carrier gas, very smooth morphologies without back-etching features can be achieved, as illustrated in Figure S4 (Supporting Information). The growth of the GaN layer on an AlN passivated $Al_{1-x}Sc_xN$ surface at high growth temperature in a nitrogen regime made the need of cleaning the reactor before the growth of the GaN layer unnecessary.

2.4. Supersaturation

The supersaturation of Ga atoms at the growing surface affects the surface morphology as well. A series of growth experiments with different supersaturation conditions has been conducted at the optimized conditions discussed in the previous section (high growth temperature, N_2 carrier gas, AlN top interlayer). The Ga molar flows was reduced from 1.2 x 10^{-4} mol min^{-1} to 3.0 x 10^{-5} mol min^{-1} to 6.1 x 10^{-5} mol min^{-1}, corresponding to high, medium and low supersaturation conditions, respectively. As shown in the AFM 90 x 90 μm scans in **Figure 4a**, a high supersaturation leads to the formation of numerous, tiny volcano-like hillocks, characterized by a several nanometer high rims and a hole in the middle. A decrease in supersaturation considerably decreases the number of these volcano-like hillocks, contributing to an overall smoother morphology, see Figure 4b. At sufficiently low supersaturation, the formation of the volcano-like hillocks is completely suppressed, as illustrated in Figure 4c.

The volcano-like features affect the electrical performance of the heterostructure, as shown in the *C–V* measurements shown in **Figure 5**. The heterostructure with the high number of volcano-like hillocks features a parasitic capacitance at low positive voltages and noisy features at negative voltages below the depletion voltage of the 2DEG that are not observed in the heterostructures with a less or no volcano-like hillocks. The n_s was in the range of 1.4 x 10^{13} cm^{-2} and R_{sh} in the range of 230 Ω/sq for all three heterostructures.

2.5. Optimization of the Interface of GaN cap and $Al_{0.94}Sc_{0.06}N$ Barrier

The successful growth of single crystalline GaN layers on $Al_{1-x}Sc_xN$/GaN heterostructures with N_2 as carrier gas and interlayers of 1 and 3 nm AlN is demonstrated by STEM and EDS

ADVANCED
SCIENCE NEWS

www.advancedsciencenews.com

ADVANCED
PHYSICS
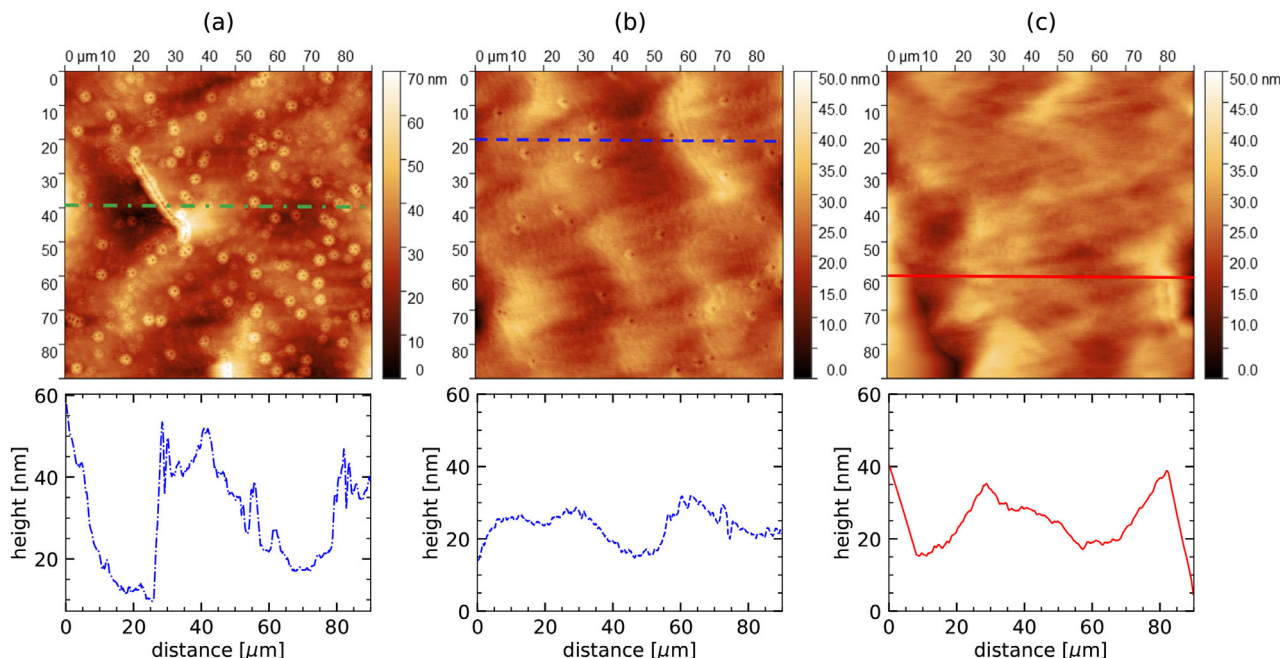**RESEARCH**
Open Access

www.advphysicsres.com

Figure 4. Surface morphology obtained by AFM of GaN caps grown under a) high, b) medium and c) low supersaturation conditions. The RMS are 8.78, 4.83, and 5.13 nm, respectively.

analyses shown in **Figure 6**. Overview and atomic resolution micrographs show 21 and 26 nm thick but atomically flat GaN caps grown uniformly across a couple of µm with the field-of-view limited by the geometric restrictions of the cross-section lamella. The investigations reveal that formerly observed Sc-rich termination layers transitioned into island-shaped impurities which are spatially separated by a 1 nm AlN layer (compare Figure 6d) but

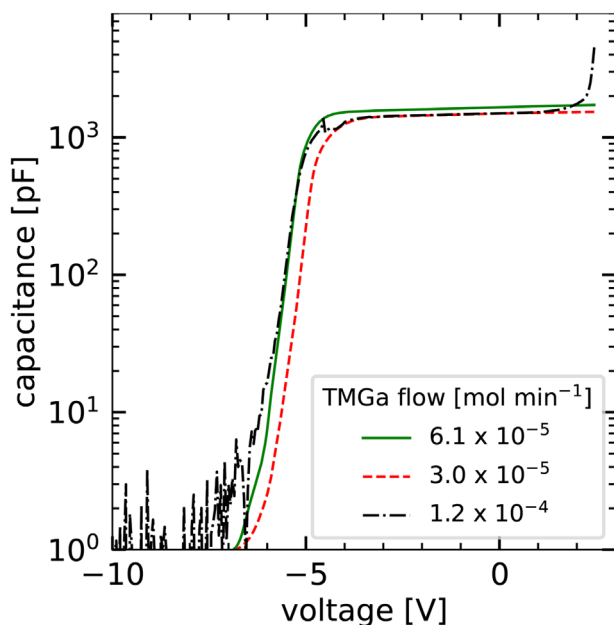seem to be overgrown completely by the AlN interlayer in case of choosing 3 nm thickness. The thicker GaN cap also successfully prevented issues with oxidation of the Sc-enriched barrier layer interface (cf., Supporting Information S3).

The structural improvement at the GaN cap/$Al_{0.94}Sc_{0.06}N$ barrier interface achieved with a nominal AlN interlayer can also be observed in HRXRD. The $\Theta/2\Theta$-scans of the 0002, 0004, and 0006 reflections of a GaN/ $Al_{0.94}Sc_{0.06}N$/GaN heterostructure and of a GaN/AlN/$Al_{0.94}Sc_{0.06}N$/GaN heterostructure are shown in **Figure 7**. The significantly increased number of thickness fringes that show up for the heterostructure grown with an AlN interlayer is indicative for a well-defined interface.

The degradation of the interface of the AlScN barrier and the GaN channel, however, becomes more pronounced for $Al_{1-x}Sc_xN$/GaN heterostructures passivated with optimized GaN caps compared to SiN_x-capped samples. The thickness of the unintentionally formed AlGaN interlayer increases. This is also visible in ToF-SIMS measurements of a $Al_{1-x}Sc_xN$/GaN heterostructures grown with a SiN_x cap and one with an optimized GaN cap that are shown in Figure S4 (Supporting Information). The high temperatures adopted for the 2D-growth of the GaN cap enhance thermal degradation in a similar way to the low growth rates that we reported on in our previous works.[31,32] This is expected to lead to enhanced alloy and interface roughness scattering at the interface and a degradation of the transport properties.

Interestingly, Hall effect measurements show the opposite. The GaN capped heterostructure has a room temperature R_{sh} of 714 Ω/sq, n_s of 8.85 x 10^{12} cm^{-2} and μ of 988 cm^2/(Vs). Under liquid nitrogen, the R_{sh} decreases to 294 Ω/sq, the charge carrier density remains approximately constant with n_s of 8.96 x 10^{12} cm^{-2} and the electron mobility μ increases to 2370 cm^2/(Vs). This unambiguously confirms the presence of a 2DEG.

Figure 5. C–V curves of GaN caps grown under high (1.2 x 10^{-4} mol min^{-1} TMGa), medium (3.0 x 10^{-5} mol min^{-1} TMGa) and low (6.1 x 10^{-5} mol min^{-1} TMGa) supersaturation conditions.

e2500035 (6 of 12)

**ADVANCED
SCIENCE NEWS**

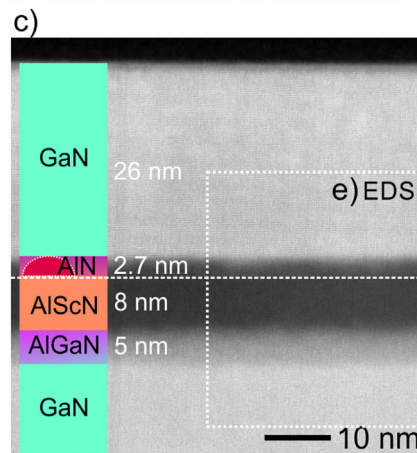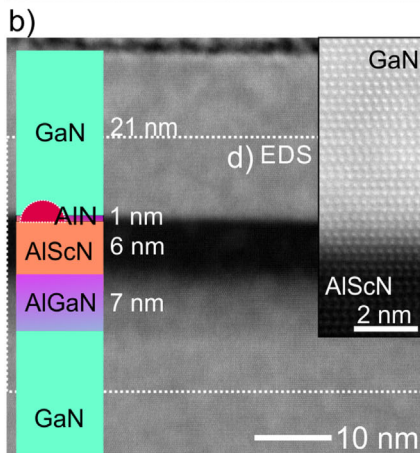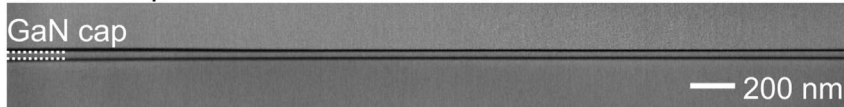www.advancedsciencenews.com

**ADVANCED
PHYSICS
RESEARCH**
Open Access

www.advphysicsres.com
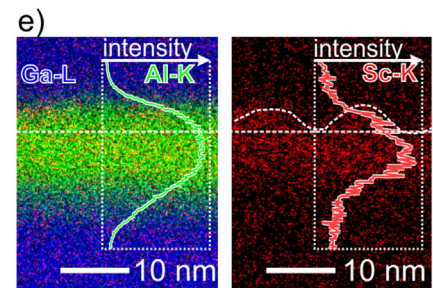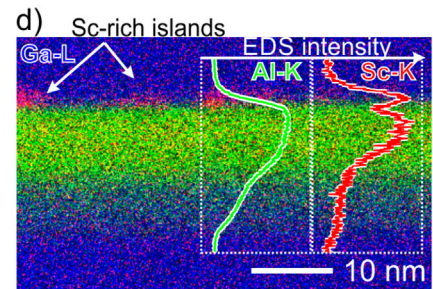
Figure 6. STEM investigation of two GaN capped $Al_{1-x}Sc_xN$/GaN heterostructures with spatial separation of the GaN cap and the $Al_{0.94}Sc_{0.06}N$ barrier by a 1 nm-thick and a 3 nm-thick AlN interlayer, respectively. a) STEM overview image shows the continuous GaN cap layer across several micrometers of the heterostructure grown with the 3 nm-thick AlN interlayer. b,d) HRSTEM and EDS analysis show the 21 nm thick single crystalline GaN cap grown onto a $Al_{1-x}Sc_xN$/GaN heterostructures with 1 nm AlN interlayer. c,e) HRSTEM and EDS analysis of $Al_{1-x}Sc_xN$/GaN heterostructures with 3 nm AlN interlayer capped by a 26 nm GaN layer. Despite the AlN interlayer, nanoscale Sc-rich islands are identified by EDS, which are overgrown in case of a 3 nm AlN layer.

A $Al_{1-x}Sc_xN$/GaN heterostructures with the same AlScN layer thickness and Sc concentration as the GaN cap one but with a SiN_x cap had a room temperature R_{sh} of 260 Ω/sq, n_s of 3.85 x 10^{13} cm^{-2} and μ of 634 cm^2/(Vs). Under liquid nitrogen, the R_{sh} decreased to 126 Ω/sq, while charge carrier density remained approximately constant with n_s of 3.65 x 10^{12} cm^{-2} and the electron mobility μ increased to 1170 cm^2/(Vs).

The transport properties of GaN-capped heterostructures are hence distinctly different from those of AlScN heterostructures passivated with SiN_x.

2.6. AlYN

For the growth of an GaN/$Al_{0.92}Y_{0.08}$N/GaN heterostructure, the information obtained on GaN/$Al_{0.94}Sc_{0.06}$N/GaN heterostructures was implemented, such as a growth interruption between the barrier and the capping layer and an increased growth temperature of the cap (1180°C) with respect to the barrier (1100°C).

Two $Al_{0.92}Y_{0.08}$N/GaN heterostructures are analyzed in this section: one capped with SiN_x and one with a GaN cap. Interestingly, the growth temperature required to achieve a bi-dimensional
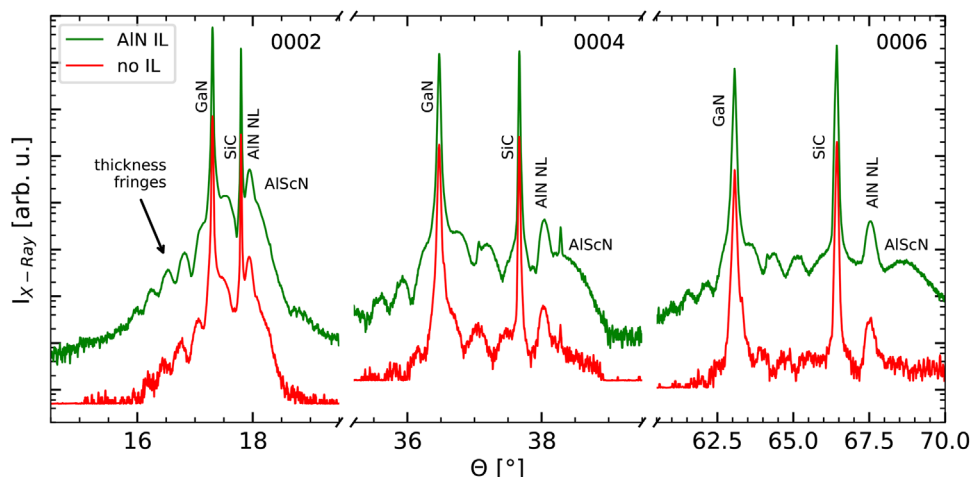

Figure 7. HRXRD Θ/2Θ-scans of the 0002, 0004, and 0006 reflections of a GaN/$Al_{0.94}Sc_{0.06}N$/GaN heterostructure and a GaN/AlN/$Al_{0.94}Sc_{0.06}N$/GaN heterostructure. The insertion of the AlN interlayer between the GaN cap and the $Al_{0.94}Sc_{0.06}N$ barrier increases the number of thickness fringes significantly.

ADVANCED
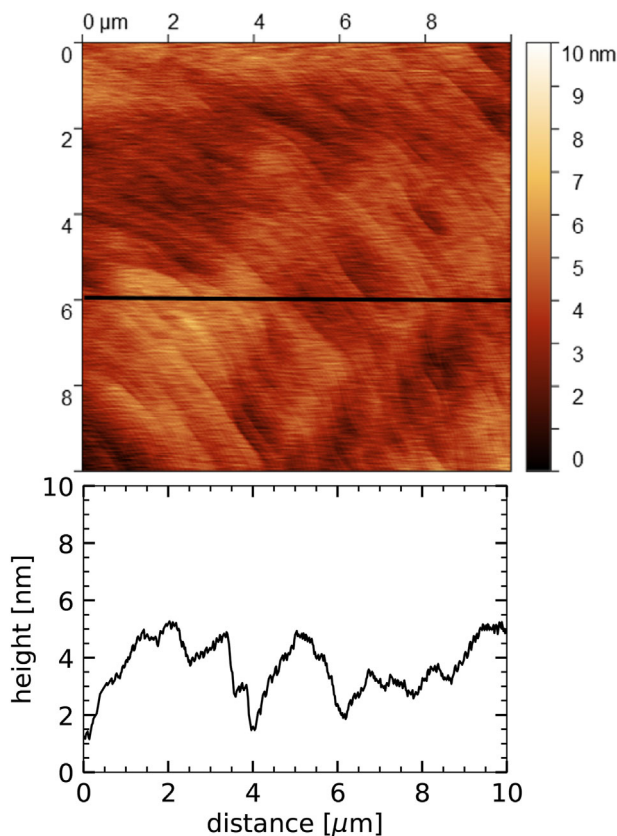SCIENCE NEWS

www.advancedsciencenews.com

ADVANCED
PHYSICS
RESEARCH
Open Access

www.advphysicsres.com

Figure 8. AFM image (10x10 μm^2 scan) of a $Al_{1-x}Sc_xN/GaN$ heterostructures with a GaN cap grown with N_2 as carrier gas. The RMS is 0.88 nm.

growth of the GaN layer was already reached at 1180°C. The surface roughness of this GaN cap is examined by AFM showing a height difference of about 3 nm. No GaN islands formation is observed, as shown in **Figure 8**.

The lower thermal budget led to a slightly better defined barrier/channel interface of the $Al_{1-x}Y_xN/GaN$ than the one observed for $Al_{1-x}Sc_xN/GaN$ heterostructures, as shown in the ToF-SIMS measurement in Figure S6 in the supporting information. Excellent performance of $Al_{1-x}Y_xN/GaN$ capped with SiN_x was observed in C-V measurements, as we showed in our previous work.[5] Contactless Hall effect measurements revealed a R_{sh} of 403 Ω/sq, a n_s of 1.37 x 10^{13} cm^{-2} and a μ of 1139 cm^2/(Vs).

Contactless Hall effect measurements of the GaN-capped heterostructure resulted in a R_{sh} of 369 Ω/sq, a n_s of 1.32 x 10^{13} cm^{-2} and a μ of 1280 cm^2/(Vs). C-V measurements were not successful. However, it is worth stressing that, due to the not very high growth temperature needed for the GaN cap on AlYN, the transport properties were not altered by changing the capping layer, as in the case of AlScN heterostructures.

Figure 9a presents the HAXPES spectra of the $Al_{0.92}Y_{0.08}N$ barrier layer capped by a layer of 10 nm SiN, measured at photon energies of 2.8 keV and 6 keV. The 2.8 keV measurement provides information on the $Al_{0.92}Y_{0.08}N$ layer near the $SiN_x/Al_{0.92}Y_{0.08}N$ interface due to its limited information depth, whereas the 6 keV measurement has a larger information depth, revealing more about the underlying $Al_{0.92}Y_{0.08}N$ layer.

In the 2.8 keV (interface-sensitive) spectra, the Al 2s peak feature is below the detection limit, while in the 6 keV spectra, the Al 2s peak is well pronounced. The Y 3p peaks are visible in both the 2.8 and 6 keV spectra, with no significant change in peak intensity.

Once more, the observed intensity variations cannot be attributed to changes in photoionization cross-sections at different core levels and excitation energies. Both Y 3p and Al 2s exhibit comparable decreases in cross-section by approximately a factor of 1/7.6 and 1/7.7 with increasing the excitation energy to 6 keV.[33] For a homogeneous $Al_{0.92}Y_{0.08}N$ layer, a similar intensity scaling for both Y 3p and Al 2s is expected. However, as this is not observed, the chemical distribution within the $Al_{0.92}Y_{0.08}N$ layer is expected to be not uniform. Instead, an enrichment of Y at the $SiN/Al_{0.92}Y_{0.08}N$ interface is assumed.

The investigation of the nanostructure and chemical properties of a GaN capped $Al_{0.92}Y_{0.08}N/Al_{1-x}Ga_xN/GaN$ heterostructure by STEM is presented in Figure 9b,c. The 2D growth of an 6.5 nm thin all-epitaxial and c-axis directed M-polar GaN capping layer onto a nominally $\approx$ 8 nm thin $Al_{0.92}Y_{0.08}N$ barrier layer is demonstrated. Chemical analysis by STEM-EDS reveals lateral and vertical yttrium clustering within the film forming columnar arrangements with $\approx$ 3–4 nm width as well as a $\approx$ 1.5 nm interlayer in which Y is absent at the interface to adjacent $Al_{1-x}Ga_xN/GaN$ layers. The relative cation composition in Y-rich regions is determined to be $x = 0.14$ and $x = 0.06$ in Y-poor regions. Moreover, only the Y-signal from Y-enriched columns extends into the GaN capping layer, providing evidence of a Y-enriched interface as confirmed by HAXPES. The non uniform distribution of Y in the layer is most likely caused by a not-constant supply of Y during the growth process. not-optimized set-up for the heating of the Y-source. Probably, the yttrium clusters are responsible for the unsuccessful C–V measurements. They offer leakage paths through the dielectric barrier layer.

3. Discussion

The growth of smooth and crystalline GaN caps in $Al_{1-x}Sc_xN$ is challenging, as GaN tends to form islands when grown in layers containing Sc.[21,30] It seems that the low Ga adatom mobility on Sc-containing layers results in the formation of GaN islands, as shown in Figure 2. The surface energy of an initially layer-by-layer grown film changes and the bond between the adsorbing atoms and the layer becomes weaker than the bonds between the adsorbed atoms and island growth is favored for the following adsorbed atoms.

We found that two-dimensional, highly crystalline GaN layers can be grown on $Al_{1-x}Sc_xN$ by combining the following approaches:

- Increase the surface mobility of the Ga atoms by increasing the GaN cap growth temperature.
- Low supersaturation to keep the growth rate low and to allow for the Ga atoms to settle before others arrive.
- Nitrogen as carrier gas to avoid backetching of the cap during its growth.
- Spatial separation of the GaN cap and the $Al_{1-x}Sc_xN$ barrier by operating desorption steps during growth and inserting an AlN interlayer between the $Al_{1-x}Sc_xN$ layer and the GaN cap.

e2500035 (8 of 12)
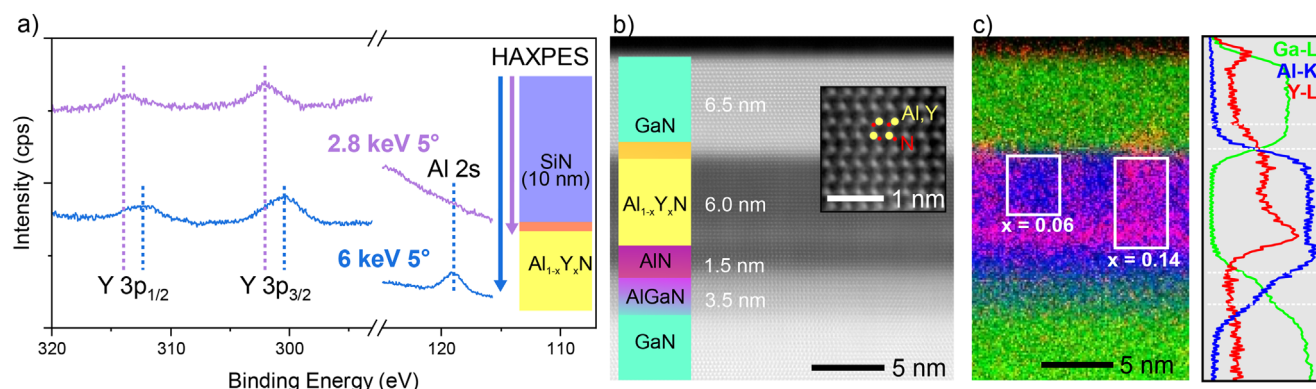
**ADVANCED
SCIENCE NEWS**

www.advancedsciencenews.com

**ADVANCED
PHYSICS
RESEARCH**

www.advphysicsres.com

Figure 9. HAXPES and STEM analysis of $Al_{0.92}Y_{0.08}N$ barrier layers capped by SiN_x and GaN. a) HAXPES spectra of an $Al_{0.92}Y_{0.08}N$ layer with a 10 nm SiN_x capping layer. b) HRSTEM micrograph of the entire $Al_{0.92}Y_{0.08}N$ based heterostructure showing the individual layers which can be discriminated by their Z-contrast. The inset confirms consecutive M-polar growth of the $Al_{0.92}Y_{0.08}N$ layer. c) STEM-EDS map shows the spatial elemental distribution of Al, Y and Ga across the heterostructure.

An oversupply of Ga atoms at high surface supersaturation conditions favors volcano-like hillocks.

The fact that the growth temperature of the GaN cap is with 1280°C considerably above the growth temperature of the $Al_{0.94}Sc_{0.06}N$ barrier with 1100°C leads to the formation of a several nm-thick, compositional graded interlayer. This was expected to cause a degradation of the 2DEG transport properties in terms of alloy and interface roughness scattering but in fact increased the electron mobility. Probably, this is due to the decrease in the sheet charge carrier density caused by the GaN cap which pulls the conduction band edge upward, above the Fermi level and reduces the depth of the potential well.[23] Lower n_s reduces electron-electron scattering and unlocks higher electron mobilities. Apart from the interface degradation, no compositional or structural degradation is observed for $Al_{1-x}Sc_xN$. The investigated $Al_{1-x}Y_xN$ barrier with GaN cap, in contrast, suffers from lateral and vertical Y inhomogeneity across the layer. As stated above, this inhomogeneity is connected to the unstable supply of the solid precursor. The fact that $Al_{1-x}Y_xN$/GaN capped with SiN_x discussed in our previous work were shown to have excellent $C-V$ characteristics,[5] while the heterostructure grown in the same way but with a GaN cap does not, suggests that some thermal degradation occurred. Most likely this was facilitated by the high growth temperature required for the deposition of the GaN layer.

In our current reactor setup, we encounter an additional challenge: the distance of the Sc precursor inlet valve and the reactor chamber causes a delay in turning off the low vapor pressure precursor flow, especially when elevated flows are operated. In our earlier work,[31] we observed that Sc incorporated into the SiN_x capping layer and degraded the electrical properties of the heterostructure, but could be largely removed by purging the gas lines and reducing the gas inlet temperature for the growth of the SiN_x cap. With STEM and HAXPES, we observed that residual Sc or Y still arrive from the gas line and lead to the formation of a Sc- or Y-rich terminating layers at the top of the $Al_{1-x}Sc_xN$ or $Al_{1-x}Y_xN$ barrier. The Sc-rich layer was reduced to single, Sc-enriched islands by removing excess Sc with desorption steps and counterbalancing it with an Al excess with an AlN interlayer before the growth of the GaN cap. The impact these Sc-rich regions might

have on the electrical performance of devices is currently under investigation.

The STEM analysis shows that no oxidation of the $Al_{0.94}Sc_{0.06}N$ barrier takes place when the GaN cap is sufficiently thick (Supporting Information S2). High thickness of the GaN cap is, however, associated to the formation of a 2D hole gas in the GaN cap. Calculations of the conduction and valence band edges with the compositional information obtained by HRSTEM and ToF-SIMS suggest that the 20 nm-thick GaN cap layer of the optimized $GaN/Al_{0.94}Sc_{0.06}N/GaN$ heterostructure causes the formation of 2DHGs in the capping layer, close to the interface with the $Al_{0.94}Sc_{0.06}N$ barrier, as illustrated in **Figure 10a,b**. The 2DEG spreads across the thermal budget-induced compositional grading at the interface of $Al_{0.94}Sc_{0.06}N$ barrier and GaN channel. The simulated electron density in the 2DEG $n_{s, sim}$ is 3.71×10^{13} cm^{-2} while the simulated hole density in the 2DHG $p_{s, sim}$ is 3.16×10^{13} cm^{-2}. The difference of these two charge components is with 5.5×10^{12} cm^{-2} in the range of the n_s determined by Hall effect measurements (8.85×10^{12} cm^{-2}). Also the $GaN/Al_{0.92}Y_{0.08}N/GaN$ heterostructure features a 2DHG according to the simulations, as shown in Figure 10c,d. Here, the simulated electron density in the 2DEG $n_{s, sim}$ is 1.95×10^{13} cm^{-2} while the simulated hole density in the 2DHG $p_{s, sim}$ is 5.58×10^{12} cm^{-2}. This results in net sheet charge carrier density of 1.39×10^{13} cm^{-2}. This matches n_s determined by Hall effect measurements well (1.37×10^{12} cm^{-2}). A decrease in GaN cap thickness lowers the net polarization at the cap/barrier heterojunction and pushes the valence band below the Fermi level, removing the 2DHG. The GaN cap thickness can be decreased by reducing the growth duration while operating the optimized growth conditions. Oxidation was observed to affect the first 3–5 nm of the GaN layer, which makes this the recommended minimum thickness.

Most recently demonstrated $GaN/Al_{1-x}Sc_xN/GaN$ heterostructures grown by MBE had a 2 nm-thick GaN cap. Nomoto et al.[34] achieved a R_{sh} of 573 Ω/sq and a n_s of 2.20×10^{13} cm^{-2} with a $GaN/Al_{0.94}Sc_{0.14}N/GaN$ heterostructure, while El Whibi et al.[35] showed 690Ω/sq and 1.60×10^{13} cm^{-2} for a $GaN/Al_{0.95}Sc_{0.15}N/GaN$ heterostructure. The thicker the GaN cap, the more the conduction band edge is pulled upward and the

**ADVANCED
SCIENCE NEWS**

www.advancedsciencenews.com

**ADVANCED
PHYSICS
RESEARCH**
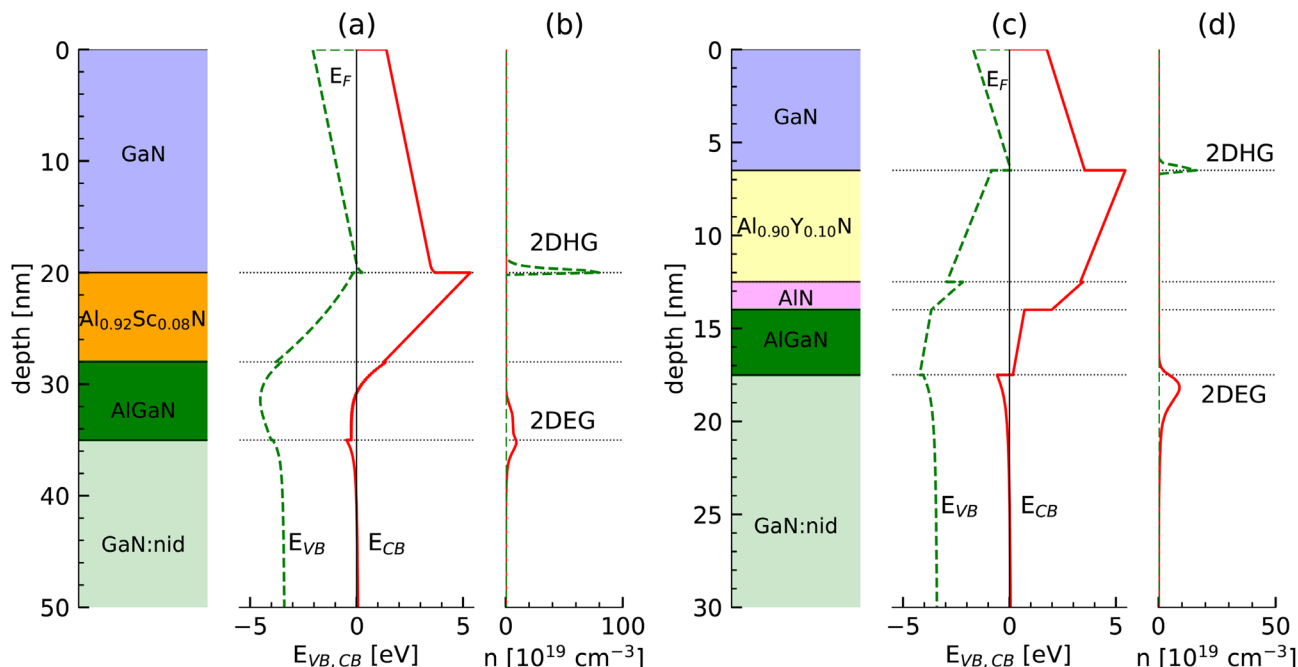Open Access

www.advphysicsres.com

Figure 10. The 1D Schrödinger–Poisson simulations of a) the conduction and valence band edges and b) charge carrier distributions of the optimized GaN/AlScN/GaN heterostructure and c) the conduction and valence band edges and d) charge carrier distributions of the optimized GaN/AlYN/GaN heterostructure show 2DHGs in the GaN caps and 2DEGs in the GaN channels.

shallower the potential well where the 2DEG is formed. Consequently, the n_s is lower, the thicker the GaN cap is. The MOCVD-grown, optimized GaN/Al$_{0.94}$Sc$_{0.06}$N /GaN heterostructure with a 26 nm-thick GaN cap that was discussed earlier has an n_s of 8.85×10^{12} cm^{-2}, with a R_{sh} of 714 Ω/sq. With the reduction of the GaN cap thickness to 3 nm, a n_s of 1.94×10^{13} cm^{-2}, with a R_{sh} of 502 Ω/sq was achieved with a MOCVD-grown, lattice-matched GaN/Al$_{0.89}$Sc$_{0.11}$N/GaN heterostructure. The μ of this heterostructure is with of 643 cm^2/(Vs) higher than the 494 cm^2/(Vs),[34] and 596 cm^2/(Vs)[35] achieved by MBE at a similar n_s.

4. Conclusion

MOCVD growth of single crystalline and homogeneous GaN capping layers has been demonstrated onto Al$_{0.94}$Sc$_{0.06}$N and Al$_{0.92}$Y$_{0.08}$N barrier layers to eliminate surface oxidation during transistors processing. The formerly observed GaN island growth was found to be connected to the low surface mobility of Ga atoms on Al$_{1-x}$Sc$_x$N and Al$_{0.92}$Y$_{0.08}$N surfaces. Smooth surfaces were achieved by increasing the surface mobility of the Ga atoms with higher growth temperatures and decreased the surface supersaturation. Interestingly, the required increase of GaN growth temperature was not as high, when the GaN was deposited on AlYN, probably due to a lower interaction between the Y and the Ga atoms on the growing surface. Based on the results of in-depth structure and chemical investigations using the analytical synergy of both STEM and HAXPES, the impact of the identified Sc-rich surface termination layer of Al$_{1-x}$Sc$_x$N barrier layers could be reduced by the deposition of AlN interlayers at higher temperature, supporting the homogeneous and 2D overgrowth of GaN caps. Growing the GaN cap too thick is expected to result in the

formation of a 2D hole gas in the GaN cap with yet unexplored consequences for the electrical performance of devices. The presented results demonstrate pivotal achievements in the development of novel HEMTs based on Al$_{1-x}$Sc$_x$N and Al$_{1-x}$Y$_x$N barrier layers.

5. Experimental Section

Al$_{1-x}$Sc$_x$N/GaN and Al$_{1-x}$Y$_x$N/GaN heterostructures with GaN caps were grown in a close coupled showerhead MOCVD reactor equipped with a proprietary heated gas injection system, which was previously developed for precursors with low vapor pressure.[17,36] The heterostructures were grown on 4-inch c-plane Al$_2$O$_3$ substrates with Fe-doped and unintentionally doped GaN buffer layers.[37] One Al$_{1-x}$Sc$_x$N/GaN heterostructures was grown with a standardized in-situ SiN$_x$ cap grown at 1100°C for comparison. The choice of the appropriate Sc and Y precursors affects the growth process and performance of Al$_{1-x}$Sc$_x$N/GaN heterostructures and Al$_{1-x}$Y$_x$N/GaN.[5,31,32] The Sc precursors selected for the deposition of the Al$_{1-x}$Sc$_x$N layers presented in this work were bis-(ethylcyclopentadienyl) (N,N'- bis (dimethylamino) acetamidinato) scandium (EtCp)$_2$Sc(bdma) or bis(ethyl cyclopentadienyl) (di-tert-butyl-triazenido)scandium (EtCp)$_2$Sc(dtbt) while tris-methylcyclopentadienylyttrium (MCp)$_3$Y was used as Y precursor. They were supplied by Dockweiler Chemicals GmbH.[38] Trimethylaluminum TMAl, trimethylgallium TMGa, silane SiH$_4$ and ammonia NH$_3$ were used as sources for Al, Ga, Si, and N, respectively. The carrier gas chosen for the growth of the heterostructures was hydrogen, only for the growth of the GaN cap also nitrogen was employed. A Sc concentration of 6% slightly below the lattice-matched concentration was chosen for most of the 10 nm-thick Al$_{1-x}$Sc$_x$N barriers. The lower the Sc concentration the higher the n_s.[39] At Sc concentrations below the lattice-matched one in-plane tensile strain adds piezoelectric polarization to the spontaneous polarization of the barrier and increases the total polarization difference at the interface to the GaN channel. Consequently the n_s in the 2DEG

increases. One lattice-matched GaN/Al$_{0.89}$Sc$_{0.11}$N/GaN heterostructure was grown as well.

The GaN cap on Al$_{1-x}$Sc$_x$N/GaN heterostructures was optimized using two approaches: First, the optimization of the layer sequence by inserting AlN interlayers between the barrier layers and the GaN caps and by inserting growth interruptions. Second, the growth parameters during GaN cap growth were adjusted. The growth temperatures of the GaN cap (T$_{GaN}$), the carrier gas (H$_2$, N$_2$) and the supersaturation were varied. The latter is intertwined with the growth rate. Finally, the optimized GaN cap was grown also on Al$_{1-x}$Y$_x$N/GaN. The growth temperature of this cap was 1180°C while that of the AlYN barrier was at 1100°C.

Depth profiles of the chemical composition of the Al$_{1-x}$Sc$_x$N/GaN heterostructures and Al$_{1-x}$Y$_x$N/GaN were determined using time-of-flight secondary ion mass spectrometry (ToF-SIMS) and can be found in the supporting information. The AlCs$^+$/ScCs$^+$ signal ratio were compared to that of magnetron-sputtered AlScN reference samples in order to determine the Sc concentration. These reference samples were previously calibrated by energy elastic recoil detection analysis (ERDA).[40] High-resolution X-ray diffraction (HRXRD) Θ/2Θ-scans of the 0002, 0004 and 0006 reflection ranges was combined with X-ray reflectometry (XRR) to determine the barrier (th$_{barrier}$) and cap (th$_{cap}$) layer thicknesses and HRXRD reciprocal space mappings (RSM) of the $\bar{1}\bar{1}$24-reflection ranges were employed to confirm that the AlScN barriers and the GaN caps are coherently strained to the underlying GaN. The morphology including the root mean square roughness (RMS) of the heterostructures was examined both by differential interference contrast microscopy (DIC) and atomic force microscopy (AFM) in tapping mode. The electrical performance of the 2DEGs of was analyzed with contactless eddy-current sheet resistance and contactless Hall measurements at room temperature. Average values for sheet resistance (R$_{sh}$), sheet charge carrier density (n$_s$) and electron mobility (μ) were determined by measuring 17 points evenly distributed across the 4 inch wafers. Additionally, Hall measurements were conducted with alloyed Ti/Al-based contacts to compare R$_{sh}$, n$_s$ and μ at room temperature and at 77 K. Low field-characteristics cannot be directly related to the high-field performance of a transistor operated in the saturated regime, however they define the behavior of a transistor in the linear regime. The presence of 2DEGs was further confirmed by capacitance voltage (C-V) measurements performed with a mercury probe. Current-voltage (I-V) measurements were employed to determine the leakage currents of the mercury Schottky contacts at negative voltages to anticipate gate leakage currents in transistors.

Atomic resolution imaging of the heterostructures' cross sections and their atomic scale spectroscopic analysis was performed on a NION UltraSTEM microscope operated at 200 keV and a JEOL Neoarm microscope operated at 200 keV. High-angle annular darkfield (HAADF) imaging was used in conjunction with chemical analysis by energy-dispersive X-ray spectroscopy (EDS) and core-loss electron energy loss spectroscopy (EELS). EDS and EELS signals were acquired in parallel in a single scan.

HAXPES was performed at the P22 beamline of PETRA III (DESY, Hamburg)[41] to investigate element-selective chemical properties. Core level spectra of Al, Sc, Y, and N were recorded at photon energies of 2.8 keV and 6 keV, providing an information depth of 9 nm and 18 nm, respectively. HAXPES is therefore more depth sensitive than conventional laboratory XPS (Al K$_\alpha$ or Mg K$_\alpha$), which is typically in the range of a few nanometers.[43] A SPECS PHOIBOS 225HV electron analyzer was used at an emission angle of 5° and a pass energy of 50 eV, resulting in an overall energy resolution of approximately 300 meV.

The conduction and valence band edges as well as the theoretical charge carrier distributions of electrons and holes shown in this work were calculated with the 1D Schrödinger-Poisson equation solver nextnano^{++}.[42]

Supporting Information

Supporting Information is available from the Wiley Online Library or from the author.

Conflict of Interest

The authors declare no conflict of interest.

Data Availability Statement

The data that support the findings of this study are available from the corresponding author upon reasonable request.

[1] F. Roccaforte, P. Fiorenza, G. Greco, R. Lo Nigro, F. Giannazzo, F. Iucolano, M. Saggio, *Microelectron. Eng.* **2018**, *187–188*, 66.

[2] M. Meneghini, C. de Santi, I. Abid, M. Buffolo, M. Cioni, R. A. Khadar, L. Nela, N. Zagni, A. Chini, F. Medjdoub, G. Meneghesso, G. Verzellesi, E. Zanoni, E. Matioli, *J. Appl. Phys.* **2021**, *130*, 181101.

[3] J. A. Del Alamo, E. S. Lee, *IEEE Trans. Electron Devices* **2019**, *66*, 4578.

[4] O. Ambacher, B. Christian, M. Yassine, M. Baeumler, S. Leone, R. Quay, *J. Appl. Phys.* **2021**, *129*, 204501.

[5] I. Streicher, P. Straňák, L. Kirste, M. Prescher, S. Müller, S. Leone, *APL Mater.* **2024**, *12*, 051109.

[6] J. Casamento, H. Lee, T. Maeda, V. Gund, K. Nomoto, L. van Deurzen, W. Turner, P. Fay, S. Mu, C. G. Van de Walle, A. Lal, H. G. Xing, D. Jena, *Appl. Phys. Lett.* **2022**, *120*, 152901.

[7] N. Afshar, M. Yassine, O. Ambacher, *Front. Mater.* **2025**, *12*.

[8] S. Krause, I. Streicher, P. Waltereit, L. Kirste, P. Bruckner, S. Leone, *IEEE Electron Device Lett.* **2023**, *44*, 17.

[9] D. V. Dinh, J. Lähnemann, L. Geelhaar, O. Brandt, *Appl. Phys. Lett.* **2023**, *122*, 152103.

[10] T.-S. Nguyen, N. Pieczulewski, C. Savant, J. J. P. Cooper, J. Casamento, R. S. Goldman, D. A. Muller, H. G. Xing, D. Jena, *APL Mater.* **2024**, *12*, 101117.

[11] R. Kumar, G. Gopakumar, Z. U. Abdin, M. J. Manfra, O. Malis, *Appl. Phys. Lett.* **2024**, *125*, 052103.

[12] D. Wang, S. Mondal, P. Kezer, M. Hu, J. Liu, Y. Wu, P. Zhou, T. Ma, P. Wang, D. Wang, J. T. Heron, Z. Mi, *Appl. Surf. Sci.* **2023**, *637*, 157893.

[13] P. Vanýsek, in *CRC handbook of chemistry and physics*. (Ed: J. R. Rumble) CRC Press, Boca Raton and London and New York, ISBN 9781032121710, **2022**, https://hbcp.chemnetbase.com/faces/documents/05_22/05_22_0001.xhtml.

[14] M. Li, K. Hu, H. Lin, V. Felmetsger, Y. Zhu, in *2022 IEEE International Ultrasonics Symposium (IUS)*. **2022**, pp. 1–3.

[15] D. Wang, D. Wang, P. Zhou, M. Hu, J. Liu, S. Mondal, T. Ma, P. Wang, Z. Mi, *Appl. Surf. Sci.* **2023**, 157337.

[16] O. Rehm, L. Baumgarten, R. Guido, P. M. Düring, A. Gloskovskii, C. Schlueter, T. Mikolajick, U. Schroeder, M. Müller, *physica status solidi (RRL) – Rapid Research Letters* **2024**.

[17] S. Leone, I. Streicher, M. Prescher, P. Straňák, L. Kirste, *physica status solidi (RRL) – Rapid Research Letters* **2023**, 2300091.

[18] W. Seifert, R. Franzheld, E. Butter, H. Sobotta, V. Riede, *Cryst. Res. Technol.* **1983**, *18*, 383.

[19] C. G. van de Walle, C. Stampfl, J. Neugebauer, M. D. McCluskey, N. M. Johnson, *MRS Internet J. Nitride Semicond. Res.* **1999**, *4*, 890.

[20] A. J. E. Rowberg, S. Mu, C. G. van de Walle, *J. Appl. Phys.* **2024**, *135*, 12.

[21] C. Manz, S. Leone, L. Kirste, J. Ligl, K. Frei, T. Fuchs, M. Prescher, P. Waltereit, M. A. Verheijen, A. Graff, M. Simon-Najasek, F. Altmann, M. Fiederle, O. Ambacher, *Semicond. Sci. Technol.* **2021**, *36*, 034003.

[22] M. B. Tahhan, J. A. Logan, M. T. Hardy, M. G. Ancona, B. Schultz, B. Appleton, T. Kazior, D. J. Meyer, E. M. Chumbes, *IEEE Trans. Electron Devices* **2022**, *69*, 962.

[23] S. Heikman, S. Keller, Y. Wu, J. S. Speck, S. P. DenBaars, U. K. Mishra, *J. Appl. Phys.* **2003**, *93*, 10114.

[24] u. Janicki, R. Chaudhuri, S. J. Bader, H. G. Xing, D. Jena, R. Kudrawiec, *physica status solidi (RRL) – Rapid Research Letters* **2021**, *15*, 2000573.

[25] G. Greco, F. Iucolano, F. Roccaforte, *Mater. Sci. Semicond. Process.* **2018**, *78*, 96.

[26] L. Nela, M. Xiao, Y. Zhang, E. Matioli, *Appl. Phys. Lett.* **2022**, *120*, 190501.

[27] D. D. Koleske, A. E. Wickenden, R. L. Henry, *MRS Internet J. Nitride Semicond. Res.* **2000**, *5*, 273.

[28] D. Koleske, A. Wickenden, R. Henry, J. Culbertson, M. Twigg, *J. Cryst. Growth* **2001**, *223*, 466.

[29] A. M. Hinz, S. Ghosh, S. M. Fairclough, J. T. Griffiths, M. J. Kappers, R. A. Oliver, D. J. Wallis, *J. Cryst. Growth* **2023**, *624*, 127420.

[30] D. Koleske, J. Knapp, S. Lee, M. Crawford, J. Creighton, K. Cross, G. Thaler, Issues associated with the metalorganic chemical vapor deposition of ScGaN and YGaN alloys, Technical Report, **2009**.

[31] I. Streicher, S. Leone, M. Zhang, T. S. Tlemcani, M. Bah, P. Straňák, L. Kirste, M. Prescher, A. Yassine, D. Alquier, O. Ambacher, *Adv. Funct. Mater.* **2024**, 2403027.

[32] I. Streicher, S. Leone, C. Manz, L. Kirste, M. Prescher, P. Waltereit, M. Mikulla, R. Quay, O. Ambacher, *Cryst. Growth Des.* **2023**, *23*, 782.

[33] M. Trzhaskovskaya, V. Yarzhemsky, *At. Data Nucl. Data Tables* **2018**, *119*, 99–174.

[34] K. Nomoto, J. Casamento, T.-S. Nguyen, L. Li, H. Lee, C. Savant, A. L. Hickman, T. Maeda, J. Encomendero, V. Gund, T. Vasen, S. Afroz, D. Hannan, J. C. M. Hwang, D. Jena, H. G. Xing, *Appl. Phys. Express* **2025**, *18*, 016506.

[35] S. El Whibi, N. Bhat, Y. Fouzi, N. De France, J.-C. De Jaeger, Z. Bougrioua, F. Bartoli, M. Hugues, Y. Cordier, M. Lesecq, *Appl. Phys. Express* **2025**, *18*, 046501.

[36] S. Leone, J. Ligl, C. Manz, L. Kirste, T. Fuchs, H. Menner, M. Prescher, J. Wiegert, A. Žukauskaitė, R. Quay, O. Ambacher, *physica status solidi (RRL) – Rapid Research Letters* **2020**, *14*, 1900535.

[37] S. Leone, F. Benkhelifa, L. Kirste, C. Manz, S. Mueller, R. Quay, T. Stadelmann, *Phys. Status Solidi B 255*, 1700377.

[38] DOCKWEILER CHEMICALS, Dockweiler Chemicals, **2022**, https://dockchemicals.com/.

[39] I. Streicher, Ph.D. thesis, University of Freiburg, **2024**.

[40] A. Zukauskaite, G. Wingqvist, J. Palisaitis, J. Jensen, P. O. Å. Persson, R. Matloub, P. Muralt, Y. Kim, J. Birch, L. Hultman, *J. Appl. Phys.* **2012**, *111*, 093527.

[41] C. Schlueter, A. Gloskovskii, K. Ederer, I. Schostak, S. Piec, I. Sarkar, Y. Matveyev, P. Lömker, M. Sing, R. Claessen, C. Wiemann, C. M. Schneider, K. Medjanik, G. Schönhense, P. Amann, A. Nilsson, W. Drube, *AIP Conf. Proc.* **2019**, *2054*, 040010.

[42] Stefan Birner, nextnano - Software for semiconductor nanodevices, **2022**, https://www.nextnano.de/.

[43] M. Müller, P. Lömker, P. Rosenberger, M. Hussein Hamed, D. N. Mueller, R. A. Heinen, T. Szyjka, L. Baumgarten, *J. Vacuum Science Technology A* **2021**, *40*, 013215.